IEEE Access
Multidisciplinary | Rapid Review | Open Access Journal

Received March 31, 2021, accepted April 20, 2021, date of publication April 30, 2021, date of current version May 14, 2021.

Digital Object Identifier 10.1109/ACCESS.2021.3076779

Effect of Magnets Asymmetry on Stray Magnetic Flux Based Bearing Damage Detection in PMSM

VIGNESHWARAN GURUSAMY[1], (Graduate Student Member, IEEE), KUDRA H. BARUTI[1], (Student Member, IEEE), MOHSEN ZAFARANI[2], (Member, IEEE), WAI LEE[3], AND BILAL AKIN[1], (Senior Member, IEEE)

[1]Electrical and Computer Engineering Department, The University of Texas at Dallas, Richardson, TX 75080, USA
[2]ASML, Wilton, CT 06897, USA
[3]Texas Instruments, Dallas, TX 75243, USA

Corresponding author: Bilal Akin (bilal.akin@utdallas.edu)

This work was supported in part by the Semiconductor Research Corporation/Texas Analog Center of Excellence (SRC/TxACE), and in part by Texas Instruments Inc.

ABSTRACT In this paper, it is shown that stray magnetic flux is a highly reliable condition monitoring variable which is rich in motor health related information and it is superior to motor current. It is well-known that the magnetic field distribution in permanent magnet (PM) rotors exhibit asymmetry due to magnet manufacturing process. It is shown that, in addition to the clear characteristic bearing signatures, the magnet imperfections induce multiple new bearing fault signatures in the stray magnetic flux. Different than current, the signatures in stray flux are more immune to noise, consistent and independent of load and speed. It is also shown that the stray flux-based detection method can locate the faulty bearing. To justify the proposed approach, comparative simulations and experiments are carried out on a surface mounted PM synchronous motor (PMSM) and an interior permanent magnet motor (IPM) with outer raceway bearing fault and different degree of magnet field asymmetry.

INDEX TERMS Bearing fault, stray magnetic field, permanent magnet synchronous motor (PMSM), interior permanent magnet motor (IPM).

I. INTRODUCTION

Recently, the market share of permanent magnet motors in high-end applications have been increasing drastically due to its high-power density and high efficiency. This rapid and widespread deployment raises reliability concerns, particularly for mission and safety critical systems. Therefore, continuously monitoring these systems is essential to prevent unexpected shutdowns and catastrophic failures that may result in fatal accidents or significant operation loss.

Among the various faults in electric motors, bearing faults are statistically most common failure at about 41% [1]. Bearing failures are caused due to various reasons like operating environment, lubrication problems, installation errors, bearing currents, excessive heating due to rotor loss etc. The majority of bearing related failures are reported for induction motors due to their long history. The authors in [2] investigate a PM servo motor with damaged bearing from field to detect the fault which shows the bearing failures could happen in PM motors. As PM motors are relatively younger than induction machines, there is very limited data to corroborate that bearing failures could be the most common one. Most of the previously mentioned problems can occur both in PM and induction motors except excessive heating due to rotor losses. With the increase in deployment of wide band gap devices, high frequency bearing current related issues are expected to increase. The bearing failures in permanent magnet motors are not extensively studied like in induction motors. Even though most of the fault detection techniques used for induction motors can be inherited, the PM motors still need to be studied to develop reliable detection methods.

Bearing fault detection through vibration [2]-[6] and motor current signature analysis (MCSA) [6]-[11],[19] are the most extensively studied methods. Though accelerometer is one of the best candidates for mechanical faults, it is expensive and affected by environment. MCSA technique is proposed in [7] to detect bearing fault which requires complex signal processing techniques due to the poor signal to noise ratio (SNR)[9],[11]. In [9] authors proposed special-kurtosis and

The associate editor coordinating the review of this manuscript and approving it for publication was Anton Kos.

envelope analysis which uses autoregressive model to whiten the current and multiple filters to obtain the envelope to detect the fault. The work in [11] proposes noise cancellation technique to improve the reliability of signature in current. These extensive signal processing techniques increases the complexity of fault detection algorithm due to low energy bearing fault signatures. Stray magnetic field based monitoring techniques have been developed to detect various faults like broken magnet fault [12], rotor cage failure [13], stator winding fault [14], broken bar [15] in electrical motors. But it is not extensively studied for bearing fault detection. Multiple studies reported that detecting bearing related signature in stray flux is a challenging task [16], [17]. The authors in [16] concluded that electromagnetic flux based detection of bearing fault is difficult and the signatures in [17] are controversial to determine the fault. Bearing fault detection using statistical processing of stray flux was proposed in [18]. For a set of integer harmonics, the mean stray flux data of ten samples are compared with standard deviation of healthy motor to detect the fault. However, correlation of these signatures to bearing fault remain unclear since other faults could also show similar result. The studies [16]–[18] focus on induction motors and there are no studies on flux based bearing failure detection in permanent magnet motors.

In this paper, some key findings regarding bearing fault detection in permanent magnet motors are discussed in detail. The new stray flux signatures are proposed which act complementary to the characteristics bearing fault signatures. The stray flux around the motor is monitored by the fluxgate sensor on the housing. It is well known that even in brand new PM motors airgap magnetic field generated by the magnets are mostly not uniform due to variation in manufacturing process [19]. This causes the stray flux to vary with the position of magnets which can easily be measured with the fluxgate sensor by rotating the motor at constant speed. This results in magnetic pole frequency harmonics in the spectrum of healthy motor. It is shown that the vibration harmonics modulate the magnetic pole harmonics and generate bearing fault signatures in stray magnetic field of the motor along with the characteristic bearing signatures due to the electrical frequency. The findings show that the signatures in current are significantly suppressed by the closed loop control and load but the signature in flux are least affected. The proposed stray flux-based detection shows consistent signature throughout the operating region whereas MCSA could not detect bearing fault in most of the operating conditions. The proposed method is verified with finite element simulation of PM motors with varying degree of magnetization non-uniformity (3%, 10% and 20%) to create different level of asymmetry. The simulation results are validated with two different PM motors, one with 20% asymmetry in magnetic field and the other with 5% asymmetry in magnetic field. The following are the key contributions of this work:

- In addition to characteristic ones, new set of fault signatures are defined for bearing fault.
- Proposed method can also locate the faulty bearing, whether it is in the drive end or in non-drive end of shaft which is particularly useful for large motors and the ones with long stack length.
- The signature amplitude in flux are remarkably high and consistent throughout the entire operating region. Different than MCSA, it results in higher SNR and least affected by the load and closed loop control action of controller.
- Complex signal processing is not needed for fault diagnosis when there is remarkable asymmetry in between magnets.
- When the asymmetry in the magnets are not significant, characteristic signatures are remarkable but the amplitude of the proposed signatures in flux is relatively low especially under the closed loop operation. However, there isn't any reliable signature in the current under the same conditions.
- The magnitude of signature in flux are almost independent of load and speed. This is essential to set a stationary pre-defined threshold; whereas current signatures are highly operating point dependent and requires dynamic threshold.
- Even if the magnetic field has no asymmetry or reduced asymmetry, the signatures in flux due to electrical frequency can be used to detect the fault.
- The consistent signatures in stray flux facilitates the condition monitoring irrespective of operating point.

II. BEARING FAULT CHARACTERISTICS AND TRADITIONAL DETECTION METHODS

Bearing faults are mainly classified as two types: Single point defects, where the fault is localized and the rest of bearing area remain healthy, and generalized roughness where the fault is not apparent which could be due to surface roughness and deformity in bearing. The second type of fault results in vibration in broadband frequency [3] which makes the detection difficult. This work focuses only on the single point defects. This defect can be thought of as degradation in a specific location of bearing like raceways, rolling element which is a spherical ball in ball bearing or cage. This will result in vibration in a characteristic frequency based on the defect location. This characteristic frequency is the rate at which periodic impulses are generated due to the defect. Based on the defect location, this is further classified as inner raceway fault, outer raceway fault, ball fault and cage fault. The characteristics frequency for each of these faults depend on geometry of bearing and the frequency of rotation. The characteristic frequency for the various single point defects is given as [5]

$$\text{Outer race defect,} f_o = N_b \times \frac{f_r}{2}\left(1 - \frac{D_b \cos\theta}{D_p}\right) \quad (1)$$

$$\text{Inner race defect,} f_i = N_b \times \frac{f_r}{2}\left(1 + \frac{D_b \cos\theta}{D_p}\right) \quad (2)$$

$$\text{Ball defect,} f_b = \frac{D_p}{D_b} \times f_r \left(1 - \left(\frac{D_b \cos\theta}{D_p}\right)^2\right) \quad (3)$$

$$\text{Cage defect,} f_c = \frac{f_r}{2}\left(1 - \frac{D_b \cos\theta}{D_p}\right) \quad (4)$$

where N_b is the number of balls, f_r is the frequency of rotation, D_p is the pitch diameter of bearing, D_b is ball diameter and θ is the ball contact angle. Due to the impulsive nature of vibration, its harmonic spectrum is rich in harmonics. This well-defined characteristic frequency and its multiples are used to detect the bearing failure. With the help of this frequency, accelerometers and current sensors are used to detect the fault.

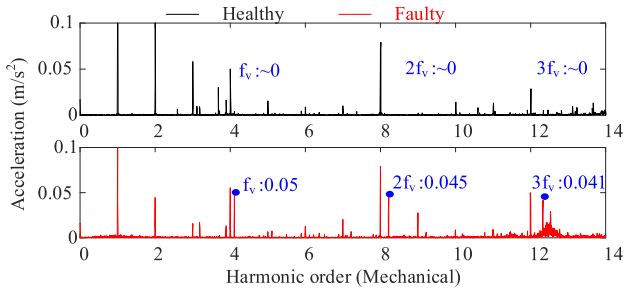

FIGURE 1. Measured vibration spectrum of a PM motor with outer race fault.

A. ACCELEROMETER BASED DETECTION

The vibration spectrum of a PM motor with outer race fault measured with industrial piezoelectric accelerometer is shown in Fig.1. The tested motor uses 6003 bearing which has theoretical outer race fault frequency order of 4.1whose fundamental frequency is rotating frequency of motor shaft. This frequency matches with the observed vibration frequency (f_v). The harmonics of the vibration frequency can also be observed in the plot. These observations are essential for the following discussions and shows the effectiveness of accelerometer in detecting the bearing fault.

B. STATOR CURRENT BASED DETECTION

Stator current based detection enables the use of existing current sensors in the drive. The vibration leads to periodic variations in winding inductances and eventually reflected in the stator current. The fault related frequency present in the stator current is the modulation of stator current frequency where carrier being the frequency of vibration. It is given as

$$f_{bng} = |kf_s \pm mf_v| \quad (5)$$

where f_{bi} is the fault frequency component in the current, k and m are integers, f_s is the electrical frequency, f_v is the characteristic frequency due to the bearing fault.

One of the major disadvantages of current based fault detection is the low magnitude of fault signatures. In some cases, this magnitude is comparable with the noise floor of the frequency spectrum which makes it highly unreliable. Hence, complex signal processing techniques might be necessary to make reliable fault decision. Most industry purpose microcontrollers have 10 to 12 bit analog to digital converter (ADC), however in order to monitor bearing related signatures in the current reliably, at least 16 bit ADC is necessary to obtain high enough resolution. Overall, the current signatures represent vibrations indirectly whereas the accelerometer measures the vibration itself directly and more accurately. These disadvantages make MCSA based bearing fault detection less attractive.

III. PROPOSED STRAY MAGNETIC FLUX BASED BEARING FAULT SIGNATURES

There are two possible physical effects of fault when ball meets the defect. The first effect is bearing fault introduces change in airgap length in the order of few micrometers [20] which depends on clearance between the balls and raceway. The airgap length of the motor with bearing fault is given as in (6) [21]

$$g(\theta, \varphi, t) = g_0 \left[1 - \alpha \cos(\theta + \varphi(t)) \sum_{k=-\infty}^{\infty} \delta\left[t - \frac{k}{f_v}\right]\right] \quad (6)$$

where g_0 is the airgap length of the motor without the fault, α is the degree of eccentricity introduced by the fault, θ is angular position of rotor, $\phi(t)$ is the angle which the defect moved, δ is the dirac delta function and f_v is the characteristic frequency of the fault. This periodical change in airgap length causes the permeance of the airgap to vary which leads to change in airgap flux density.

The second effect is variations in load torque. The increase in friction due to the defect causes the load torque to increase. As the increased torque requirement is experienced only when the ball meets the fault, it appears as periodic variation in the load torque. It is given by

$$T_m(t) = T_{Load} + T_f \cos(2\pi f_v) \quad (7)$$

where T_m is the amplitude of torque delivered by the shaft, T_{Load} is the load torque, T_f is the amplitude of bearing fault related torque and f_v is the characteristic vibration frequency. The periodic variation in torque causes the magnetomotive force (MMF) to change [21] which leads to change in airgap flux density. It is shown in [15] that the stray magnetic flux reflects the frequency characteristics of air gap magnetic field. Hence, when the airgap flux density varies, it affects the stray magnetic flux of the motor significantly.

The magnetic field generated by the magnets in PM motors are mostly not perfectly uniform with respect to each other. This asymmetry generates harmonics in magnetic pole order in the frequency domain. The measured stray magnetic flux for four healthy motors with 8 poles is shown in Fig.2(a). It can be observed from Fig.2(b) that the harmonics due to the asymmetry is present in all the tested motors but with different degree. There are number of possible reasons for this imperfection such as asymmetry in magnetization, angular

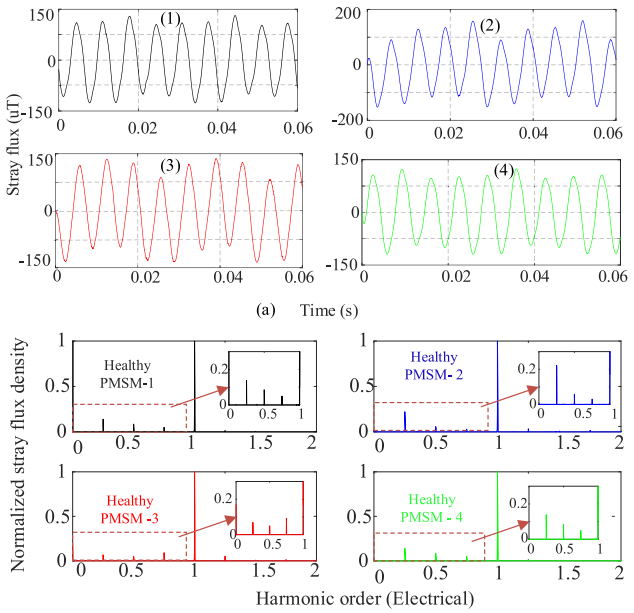

FIGURE 2. Measured stray magnetic flux of four different brand new PMSMs (a) Time domain (b) Frequency domain.

and radial disposition of magnet, rotor to stator eccentricity, variations in geometrical dimensions etc., [19].

The test motor has 8 poles which results in harmonics of order 0.25,0.5,0.75 etc., when electrical frequency of motor is considered as fundamental component. In the following sections, it is shown that these magnetic pole harmonics are modulated by the vibration harmonics and generates fault signature in stray magnetic field of motor along with the characteristic signatures generated due to fundamental electrical frequency. The fault frequencies in flux are given by

$$f_{bf} = |kf_s \pm mf_v| \tag{8}$$

where f_{bf} is the fault frequency, k and m are harmonic order which includes both fractional and integer harmonics. The outer race fault in bearing is considered for simulation and experimentation of the proposed method.

IV. MODELING AND SIMULATION

The PM motor is modeled in Ansys Maxwell 2D to study the effect of bearing failure in the stray magnetic field around the motor. The finite element model of motor is shown in Fig.3. It is a surface mount PM motor with 8 poles and 9 slots.

In the finite element model, the bearing failure is modeled as torque variation as discussed earlier which is justified with consistent experimental results. The bearing fault is modeled as pulsating torque at characteristic frequency of the fault [7], [22] as given in (7). The torque applied to the motor in the finite element model has a low ac component (1% of rated torque) at the frequency of vibration along with the dc component. It is to be noted that though the modeled torque variation is like load oscillation, torque component due to bearing fault is impulsive and has wide range of harmonics. These higher

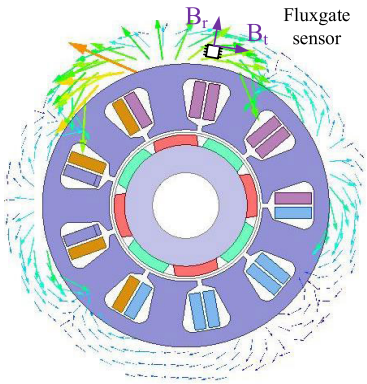

FIGURE 3. Finite element model of PMSM.

order frequencies in torque are not considered in the model in order to reduce the complexity. This assumption is reasonable since the simulation intends to show the modulation effect of fundamental vibration frequency on flux which also holds good for its harmonics. There are several parameters related to magnet dimension and manufacturing process which could result in asymmetry in magnetic field, here it is modeled as non-uniform magnetic field generated by magnets by varying their magnetization.

A. BEARING FAULT SIGNATURES IN STRAY FLUX

In order to study the effect of harmonics of magnetic pole on bearing fault, 3%, 10% and 20% variation in magnetization are considered for simulation. The three different cases are selected to show the impact of degree of non-uniformity on the fault signature. To create the asymmetry, the magnets are applied with different magnetic field intensity within the specified variation range. The harmonic order of vibration in simulation is 3.6 with the amplitude, 1% of rated torque. The order 3.6 in simulation is different from the test motor order of 4.1 to reduce the simulation time. The stray magnetic field around the motor in both the tangential (B_t) and radial (B_r) directions are monitored at a location outside the motor as shown in Fig.3.

TABLE 1. Bearing fault harmonics order - simulation.

(n) Electrical harmonic order	n+0	n+0	n+1	n+1	n+2	n+2
0.25	4.6	2.6*	8.6	1.4*	12.6	5.4*
0.5	5.6*	1.6*	9.6	2.4*	13.6	6.4
0.75	6.6	0.6*	10.6	3.4	14.6	7.4
1	7.6	0.4*	11.6	4.4	15.6	8.4

The simulated frequency spectrum of stray magnetic flux in tangential and radial direction and stator current are shown in Fig.4 to 6 for 3%, 10% and 20% non-uniformity in magnetization respectively which are plotted against the mechanical harmonic order. The fault signature order is given in Table 1 and the one in spectrum are marked with asterisk (∗). The interpretation of Table 1 is provided with the first harmonic order 4.6 as an example. Based on (8), here

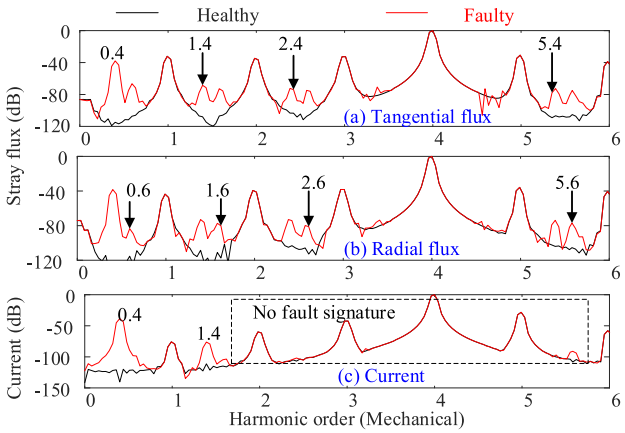

FIGURE 4. Simulation results with 3% non-uniformity. (a) Tangential stray flux spectrum (b) Radial stray flux spectrum (c) Current spectrum.

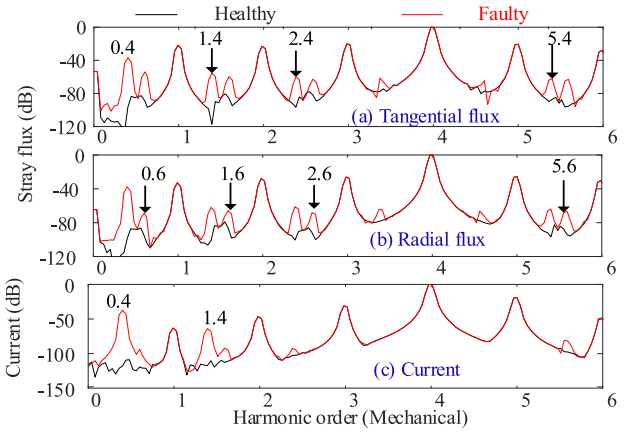

FIGURE 5. Simulation results with 10% non-uniformity. (a) Tangential stray flux spectrum (b) Radial stray flux spectrum (c) Current spectrum.

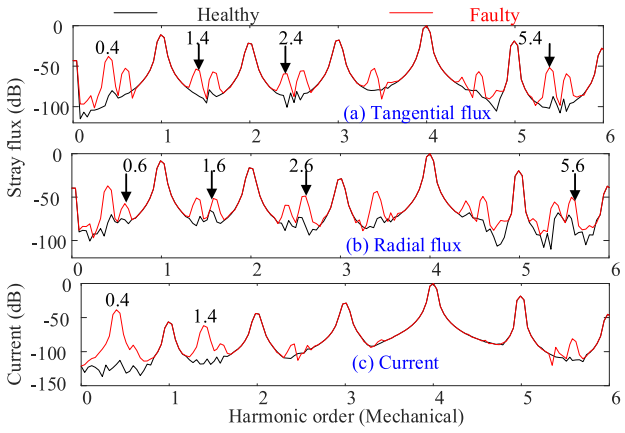

FIGURE 6. Simulation results with 20% non-uniformity. (a) Tangential stray flux spectrum (b) Radial stray flux spectrum (c) Current spectrum.

$k = n + 0 = 0.25$, $f_s = 4$, $m = 1$ since fundamental order, $f_v = 3.6$ then $f_{bf} = 4.6, 2.6$. The unshaded and shaded column of each magnetic pole harmonics order correspond to the sidebands from (8). As fundamental vibration frequency alone is considered for the simulation, Table 1 fault frequencies are related to this vibration frequency. Stray magnetic flux spectrum shows multiple fault signatures. Most of the observed fault signatures are the modulated frequencies of vibration and the magnetic pole frequency. The fault signatures are present in magnetic flux in both the radial and tangential directions. It is observed that the fault signature amplitude increases with the increase in non-uniformity. For example, the order 2.6 is about −70dB, −60dB and −50dB for 3%,10% and 20% non-uniformity cases respectively.

B. BEARING FAULT SIGNATURES IN STATOR CURRENT

The FEA simulations are performed by applying voltage to the three phase terminals of the motor. The current drawn by the motor is computed based on the operating condition. As the current signatures due to bearing fault are the modulated frequencies of vibration and the electrical frequency, it is also expected that the magnetic pole harmonics should also have impact on current signature. However, in Fig.4, 5 and 6, the fault signatures in current are mainly modulated electrical frequency. The signatures corresponding to modulated magnetic pole frequencies are almost absent in 3% non-uniformity case. In the other non- uniformity cases, some of these signatures appear with small amplitude. The magnitudes of signatures are almost the same irrespective of non-uniformity in magnets. The reason for low amplitude signature could be due to the reason that fault frequency in airgap flux causes variation in the inductances of stator winding and then it gets reflected in stator current. As mentioned in Section-II, the detection by MCSA is possible yet difficult due to low energy signatures. It can be said that the detection of fault signature in current due to the magnetic pole frequency could be challenging as well.

C. STRAY FLUX SIGNATURE ANALYSIS UNDER DIFFERENT CONDITIONS

In order to analyze the behavior of stray flux signatures, simulations are performed throughout the operating range of motor. Three-phase voltage is applied to the motor based on the operating torque and speed. Fig.7 shows the variations in some of the dominating harmonics of radial flux with respect to the speed and load current for 20% non- uniform magnetization case. The magnitude of fault signatures varies little within a small range with respect to the load and speed. The fault signature amplitudes are almost stable around −50dB to −60dB in most of the cases. The consistency in signature enables the detection of fault independent of load and speed. In the non-uniformity case of 3%, the fault signature behavior is similar to that of 20% case with reduced magnitude. The results for radial flux in this case is shown in Fig.9. The signature amplitude in this case is about −60 dB to −70 dB for most of the fault harmonics. In all the cases, the fault signature in flux are consistent irrespective of load and speed.

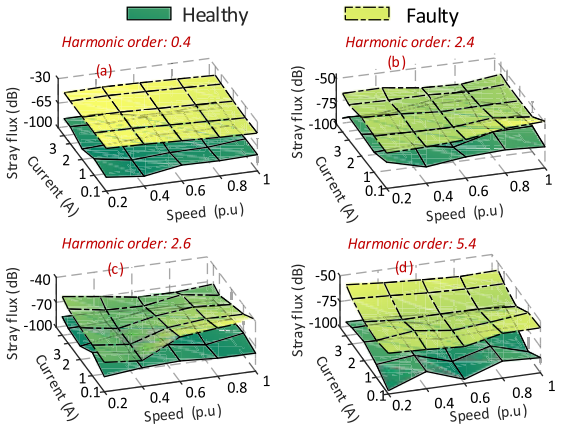

FIGURE 7. Simulation results with 20% non-uniformity: Radial stray flux.

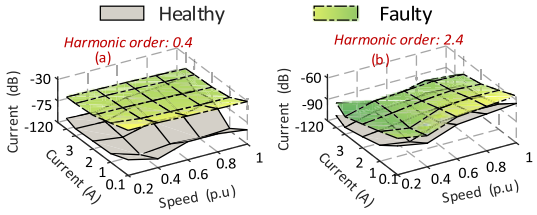

FIGURE 8. Simulation results with 20% non-uniformity: Stator current.

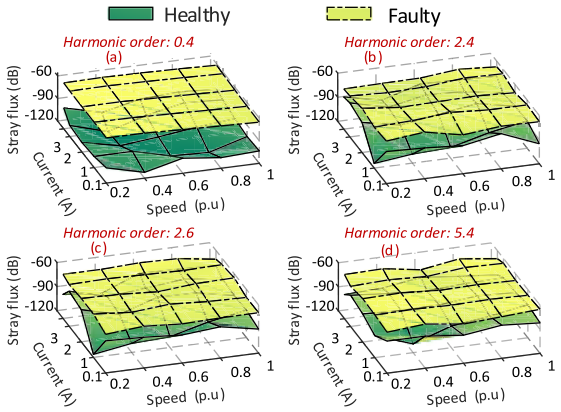

FIGURE 9. Simulation results with 3% non-uniformity: Radial stray flux.

The tangential flux also has similar characteristics in both the cases which is not shown for the sake of brevity.

D. STATOR CURRENT SIGNATURE ANALYSIS UNDER DIFFERENT CONDITIONS

As the bearing fault signatures in current are dominated by the frequencies modulated by the electrical frequency, it shows consistent behavior with the simulation throughout the full load and speed range. The results for some of the fault signature harmonics for 20% non-uniformity case are shown in Fig.8. It can be observed that the 0.4^{th} order shows very stable signature and the magnetic pole related signature 2.4 is not very stable with respect to load and speed. Though the 0.4^{th} harmonic shows stable signature, the magnitude in

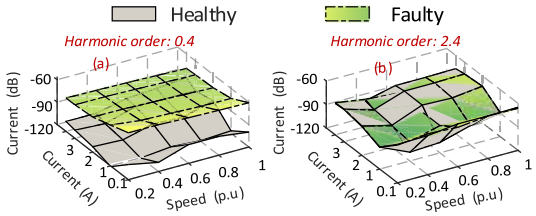

FIGURE 10. Simulation results with 3% non-uniformity: Stator current.

experiment are expected to be damped by the load inertia which is not accounted in the simulation. So, the stability of the signature cannot be ascertained with the simulation. At reduced non-uniformity case of 3%, the magnetic pole signatures are not present in current as shown in Fig.10. Based on the simulation results, it can be concluded that the stray magnetic flux shows multiple stable bearing fault signatures throughout the operating condition. The motor current does not show any stable fault signature related to magnetic pole frequency and the signatures related to electrical frequency may get affected due to damping exerted by load.

TABLE 2. Specifications of test motors.

	MOTOR-I PMSM	MOTOR-II IPM
Power in Watts	400	745
Rated current in A	2.7	3.4
Rated torque in Nm	1.27	3.95
Rated Speed in rpm	3000	1800
Number of Poles	8	6
Number of Slots	9	36

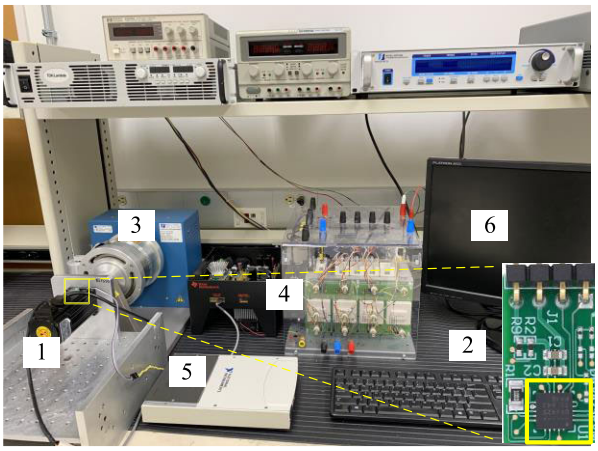

FIGURE 11. Experimental setup. (1) PMSM. (2) Fluxgate sensor (3) Dynamometer (4) Inverters (5) DAQ setup (6) PC.

V. EXPERIMENTAL RESULTS

In order to verify the simulation results, several experiments are carried out on two different permanent magnet motors with and without saliency. The first motor is a PMSM with

magnet non- uniformity of about 20% and interior permanent magnet (IPM) motor with magnet non- uniformity of about 5%. The specifications of motors are given in Table 2. The experimental setup is shown in Fig.11. The outer race of the drive end side bearing of both the motors are artificially damaged by drilling a hole. It emulates pitting at a single point which is widely adopted to validate a bearing fault diagnosis method [7], [16]–[18], [25], [26]. The test motors are connected to a hysteresis dynamometer and driven through field-oriented controlled drive. The stray flux around the motor is monitored through fluxgate sensor from Texas Instruments [22]. It is available in WQFN package with dimension 4mm × 4mm which provides the flexibility to measure flux anywhere around the motor. The sensor has resolution in the order of nT which makes it a good choice for measuring small variation in magnetic flux due to the bearing fault. The three phase stator currents are measured with LEM current sensors with a nominal current of 5A and accuracy of 1% [23]. The stray magnetic flux is measured in the axial direction using fluxgate sensor. Both the flux and current data are acquired through a data acquisition setup and further processed in MATLAB.

A. MOTOR-I WITH 20% ASYMMETRY IN MAGNETIC FIELD

The first test motor used in experiment is a PMSM with 8 poles and 9 slots same as the simulated motor.

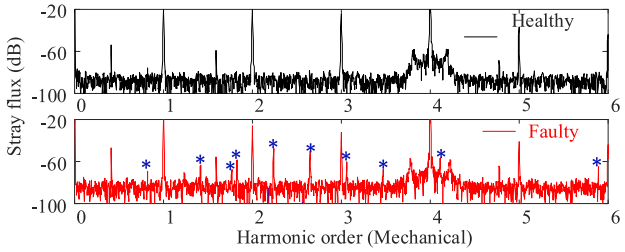

FIGURE 12. Experiment: Open loop mode– Motor-I: Stray magnetic flux spectrum.

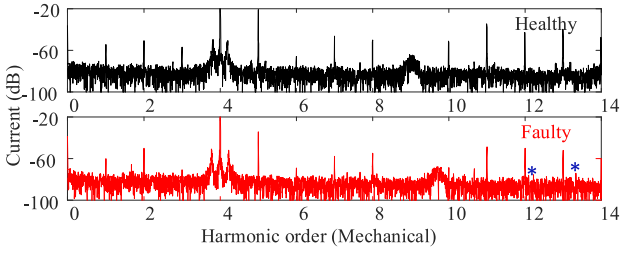

FIGURE 13. Experiment: Open loop mode– Motor-I: Current spectrum.

1) OPEN LOOP OPERATION UNDER NO LOAD

The motor is operated with the closed current loop and open speed loop under no-load. The proportional and integral gains of both the d-axis and q-axis current controllers are set equal as 1 and 0.0025 respectively. The stray flux spectrum measured in axial direction is shown in Fig.12 and the current spectrum is in Fig.13.The fault signatures are marked with an asterisk (∗). All the possible fault harmonics order are listed in Table 3 and the one observed in the experiment are in dark font. It is calculated from (8) with fs = 4 and fv = 4.1 It can be observed from the Table 3 that the subharmonics of vibration modulates the subharmonic electrical frequencies related to magnetic poles. The two set of identical electrical harmonic orders (k) in Table 3 correspond to two sideband frequencies from (8). It can be observed that, the subharmonics of vibration acts as carrier which could be due to the reason that the low frequencies are less affected by damping. Theoretically, almost all the frequencies in the Table 3 are available in stray flux spectrum. However, during the experiments many of them are below the noise level. It can be observed in the stray magnetic flux spectrum that the multiple signature related to the bearing fault exist.

TABLE 3. Bearing fault harmonics order (mechanical) of Motor-I.

Electrical harmonics order(k)	Vibration Harmonics Order (m)									
	0.1	0.2	0.3	0.4	0.5	0.6	0.7	0.8	0.9	1.0
0.25	1.41*	1.82	2.23	2.64*	3.05	3.46	3.87	4.28	4.69	5.10
0.5	2.41	2.82	3.23	3.64	4.05	4.46	4.87	5.28*	5.69	6.10
0.75	3.41	3.82	4.23	4.64	5.05	5.46*	5.87	6.28	6.69	7.10
1	4.41*	4.82	5.23*	5.64	6.05	6.46	6.87	7.28	7.69	8.10
0.25	0.59	0.18	0.23	0.64	1.05	1.46	1.87	2.28	2.69	3.10
0.5	1.59*	1.18	0.77	0.36	0.05	0.46	0.87	1.28	1.69	2.10*
0.75	2.59*	2.18	1.77*	1.36	0.95	0.54	0.13	0.28	0.69	1.10
1	3.59	3.18	2.77	2.36*	1.95	1.54	1.13	0.72	0.31	0.10

Most of the fault signatures related to fundamental frequency of magnetic pole are present in the flux spectrum. The current spectrum does not show the fault signature related to magnetic poles since the asymmetry related signatures are weaker in current. As the asymmetry related signatures are strong in flux, they are modulated by vibration harmonics resulting in multiple fault signatures. There are also fault signatures related to fundamental component of electrical frequency. This is in consistent with the simulation results in Section IV which shows many signatures related to the frequency of vibration. In the simulation many signatures are observed due to absence of mechanical damping. Similarly, in the experiment, the damping experienced by the low order frequencies is lesser than the high order vibration frequencies. The fault signature magnitudes are significant with maximum value reaching close to −40dB. The stator current spectrum has very few fault components with very low magnitude. This shows that the current signature is highly prone to noise and it is very challenging to detect the bearing failure signature in it.

2) CLOSED LOOP OPERATION UNDER NO LOAD

The motor is operated with both the closed current loop and the speed loop under no load with speed controller parameters, $k_{p\_speed} = 1$, $k_{i\_speed} = 0.005$. This is performed to see the effect of controller on the fault signatures in flux and current. PM motors are generally operated in closed loop under loaded condition. So, any fault diagnosis method must be valid for the closed loop mode in order to obtain reliable results. The measured axial stray flux spectrum is shown in Fig.14 and the current spectrum is in Fig.15. The fault signature in stray flux are different from the one in open

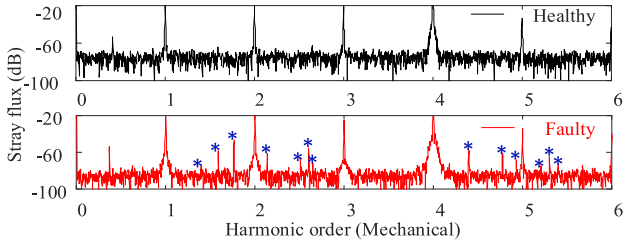

FIGURE 14. Experiment: Closed loop mode– Motor-I: Stray magnetic flux spectrum.

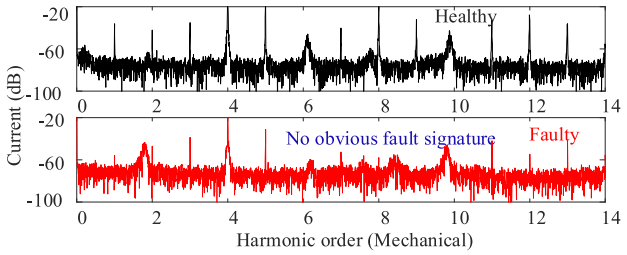

FIGURE 15. Experiment: Closed loop mode– Motor-I: Current spectrum.

loop mode. Some of the frequencies appeared in open loop mode are vanished in closed loop whereas some new fault signatures are showing up. The signatures available in closed loop are marked with asterisk (∗) in Table 3. The signatures due to both the fundamental electrical frequency and magnetic pole frequency are present in the flux. The stator current spectrum has no fault related signatures. The controller tends to suppress the fault harmonics in current [24]. The controller parameters also affect the fault signatures in both flux and current. The signatures in flux are least affected than the current [12]. The low magnitude fault signatures in the open loop mode current are completely suppressed by the controller in the closed loop operation. This shows that the current based bearing fault detection is highly unreliable.

3) CLOSED LOOP OPERATION AT DIFFERENT OPERATING CONDITIONS

It is necessary to ensure the reliability of proposed condition monitoring technique under all operating condition to facilitate continuous monitoring. This is verified by operating motor from no load to full load in its entire operating speed range. During the experiments, it is observed that some signatures appear in all the operating conditions while some are not. Some of the selected fault signature in stray flux which appear in all the operating conditions are plotted with respect to load and speed as shown in Fig.16. The fault signature order 2.6, 1.77 and 1.4 are due to magnetic pole harmonics and the order 4.4 is due to the fundamental electrical frequency. The fault harmonics of stray magnetic flux exhibit a very stable magnitude throughout the operating range. The harmonic order 2.6 changes very little with respect to the operating point and its magnitude reaches almost −50dB. The other fault harmonics vary within a small range and

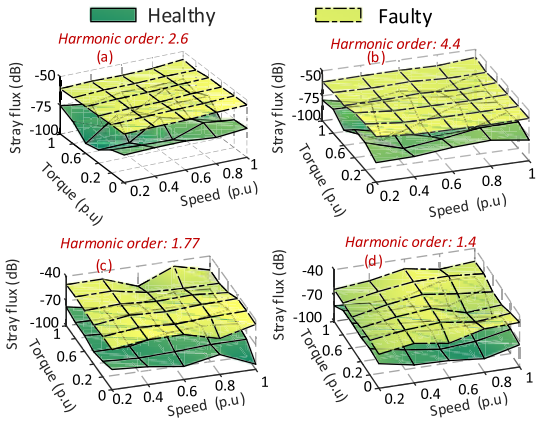

FIGURE 16. Stray magnetic flux spectrum of Motor-I in closed loop mode.

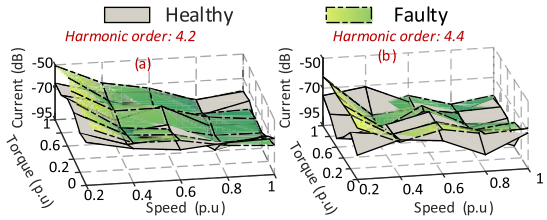

FIGURE 17. Stator current spectrum of Motor-I in closed loop mode.

have consistent amplitude throughout the torque and speed range. These results corroborate with the simulation results of stable signature throughout the operating condition. The signature in the current are not consistent with load and speed as shown in Fig.17. No single signature in current shows stable behavior with change in speed and torque.

As computationally intensive 3D simulation is required to obtain the axial stray flux, the stray flux is calculated in tangential and radial direction from 2D. The simulation results of stray magnetic flux in Fig.7 have good correlation with the experimental results in Fig.16. It can be observed that the fault signature orders are different in simulation and experiment which is due to the difference in vibration frequency as mentioned in Section IV. The fault signatures in current are suppressed due to the mechanical damping and controller. This yields some inconsistencies in current signatures in the experiments.

4) FAULTY BEARING LOCATION DETECTION

The electrical motors typically have two bearings, one at the drive end and the other at non-drive end of shaft. When MCSA is used to detect the bearing fault, it cannot provide information about the location of the faulty bearing. This information expedites the maintenance process. The stray flux-based fault monitoring utilizes the localized magnetic field which can provide insights about the fault location. In the sections *A1* to *A3*, the fluxgate sensor was placed near the drive end side which is close to the location of faulty bearing. The spectrum of axial stray magnetic flux near

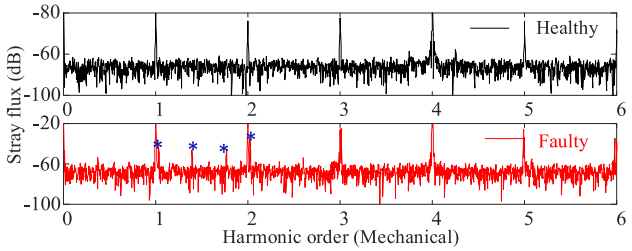

FIGURE 18. Stray magnetic flux spectrum, Motor-I open loop mode in non-drive end.

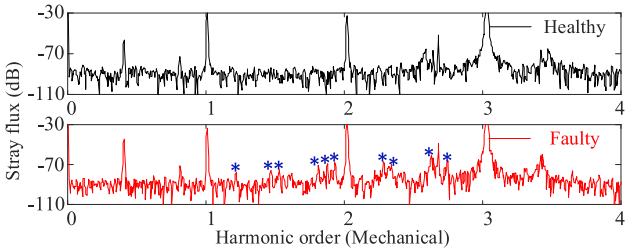

FIGURE 19. Open loop mode– Motor-II: Stray magnetic flux spectrum.

healthy bearing in open loop mode is shown in the Fig.18. It can be observed that the number of fault harmonics is lesser than the one near the faulty bearing which is shown in Fig.12. The airgap near the source of vibration varies significantly than the airgap away from source. It leads to non-uniform variation in airgap along the shaft of the motor. This results in damping of fault signature away from the faulty bearing. This variation in signature level can be used to distinguish the faulty bearing from the healthy one.

B. MOTOR-II WITH 5% ASYMMETRY IN MAGNETIC FIELD

Here, the results from Motor-II (IPM) is presented which has non-uniformity of about 5% in its magnetic field.

TABLE 4. Bearing fault harmonics order (mechanical) of Motor-II.

Electrical harmonics order(k)	Vibration harmonics order (m)									
	0.1	0.2	0.3	0.4	0.5	0.6	0.7	0.8	0.9	1
0.33	1.40	1.82*	2.21*	2.61*	3.01	3.41	3.81	4.21	4.62	5.02
0.67	2.40	2.82	3.20	3.61*	4.01	4.41*	4.81	5.21	5.62	6.02
1	3.40	3.82	4.20	4.61*	5.01	5.41	5.81	6.21	6.62	7.02
0.33	0.61	0.20	0.21	0.61	1.01	1.41	1.81*	2.22*	2.62	3.02
0.67	1.60	1.19	0.79	0.39	0.01	0.41	0.82	1.22	1.62*	2.02
1	2.60*	2.19	1.79	1.39	0.99	0.59	0.18	0.22	0.62	1.02

1) OPEN LOOP OPERATION UNDER NO LOAD

IPM motor is tested in the same experimental setup used for PMSM. During the open loop operation, the motor is run at constant speed without speed loop. Due to the absence of speed loop, the controller cannot adjust the d-axis and q-axis voltages based on the load, so the motor is run at no load. All the possible fault harmonics order are listed in Table 4 and the one observed in the experiment are in dark font. It is calculated from (7) with fs = 3 and fv = 4. The two set of identical rows in Table 4 correspond to two sideband frequencies from (7). The measured axial stray flux spectrum and the stator current spectrum are shown in the Fig.19 and 20 respectively. The fault signatures are marked with an asterisk (∗). Due to the reduced asymmetry in the magnetic field, the magnitude of signature in flux is not as significant as Motor-I. But still the signature can be discerned from the floor noise of the spectrum. The magnitude of fault signature in the current spectrum is higher than the Motor-I but it is still not superior to stray flux signature.

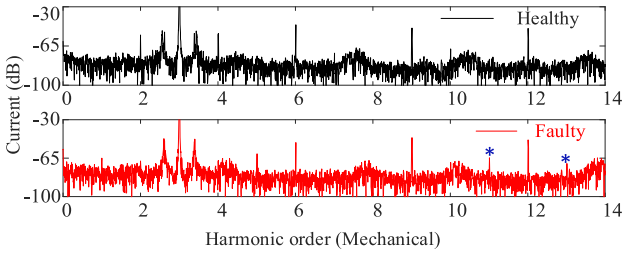

FIGURE 20. Open loop mode– Motor-II: Current spectrum.

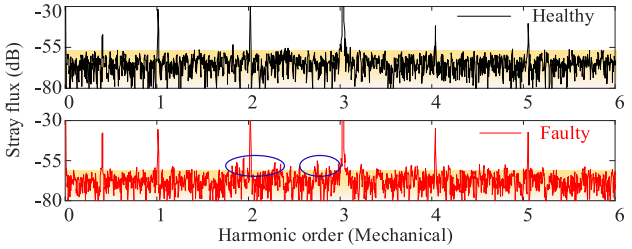

FIGURE 21. Closed loop, Motor-II: Stray magnetic flux spectrum.

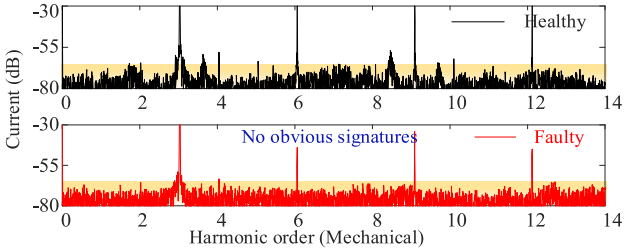

FIGURE 22. Closed loop, Motor-II: Current spectrum.

2) CLOSED LOOP OPERATION UNDER LOAD

As mentioned in A2 of this section, it is imperative that the fault signature should be consistent under closed loop operation. In order to perform tests at closed loop, the speed loop is included in the controller and motor is tested with load. The measured axial stray flux spectrum and the stator current spectrum are shown in the Fig.21 and 22 respectively. Due to the closed loop action of controller, fault signatures are suppressed in both the flux spectrum and the current spectrum. Though the current spectrum does not show any signature, flux spectrum shows some signature which are in

the encircled region in Fig.21. But the signatures are hard to differentiate from the floor noise of the spectrum. This is a typical problem of low signal to noise ratio due to the reduced amplitude of measuring signal.

To overcome this issue, spectral averaging is performed in the measured signal. Spectral averaging is a signal processing technique in which each spectral amplitude is averaged over a set of time domain signals. Here the averaging is performed with ten samples of time domain signals. This reduces floor noise significantly and improves the quality of measured spectrum. The averaged spectrum of axial stray flux and the stator current are shown in the Fig.23 and 24 respectively. The fault signatures in closed loop are highlighted in are marked with asterisk ($*$) in the Table 4. The noise floor in the averaged spectrum of stray flux has improved significantly from -80dB to about -65dB. The fault signature magnitude has become prominent with multiple fault frequencies. It can be observed that the obscure signatures in Fig.21 become clear after averaging the spectrum. The current spectrum did not show any fault related signature even after spectral averaging. These results confirm the observations in Motor-I where the current based bearing fault detection is highly unreliable and the stray flux based detection is a good alternative for PM motors.

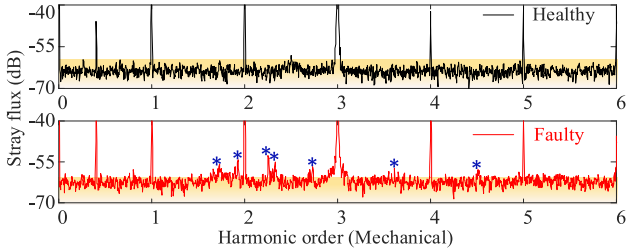

FIGURE 23. Closed loop, Motor-II – Averaged spectrum: Stray magnetic flux.

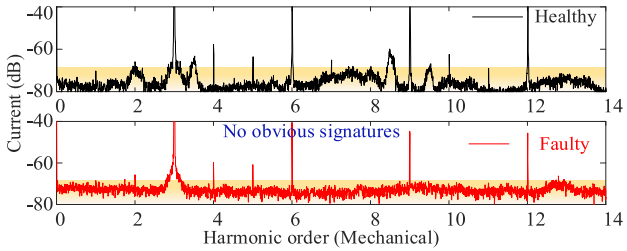

FIGURE 24. Closed loop, Motor-II – Averaged spectrum: Current.

3) CLOSED LOOP OPERATION AT DIFFERENT OPERATING CONDITIONS

The fault signatures due to the bearing need not be consistent throughout the operating range of the motor in both flux and current. This is mainly due to the low amplitude of fault signature which gets suppressed at some operating condition. The motor is operated from no load to full load throughout its speed range to verify the reliability of stray flux signature.

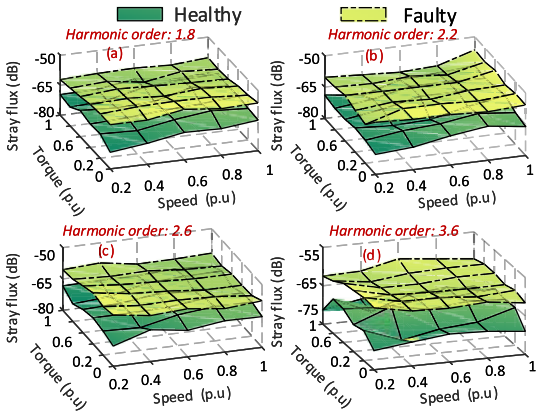

FIGURE 25. Stray magnetic flux averaged spectrum of Motor-II in closed loop mode.

As the spectral averaging provided better signature, it is adopted to obtain both the stray flux and current spectra. Some of the dominant fault signature in stray flux are plotted with respect to load and speed as shown in Fig.25. The fault related harmonics show consistent signature throughout the operating region. The magnitude of signature is about -60 dB and it changes slightly with respect to speed and torque. The fault signature order 1.8, 2.2 and 3.6 are due to magnetic pole harmonics and the order 2.6 is due to the fundamental electrical frequency. These results show the reliability of stray flux based detection and confirms the simulation data. The stator current related fault harmonics are shown in Fig.26. Though some of the fault signatures are available at low speeds, their amplitudes change randomly at higher speeds like in Motor-I.

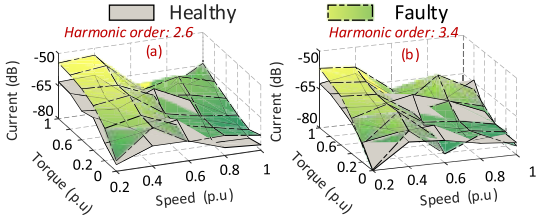

FIGURE 26. Stator current averaged spectrum of Motor-II in closed loop mode.

4) DISCUSSION AND SUMMARY OF EXPERIMENTAL RESULTS

The bearing fault signatures related to magnetic asymmetry and fundamental electrical frequency are present in stray magnetic flux spectrum. This is verified in PM motors with different level of asymmetry in magnetic field. The motor with higher level of asymmetry shows strong fault signatures than the one with reduced level of asymmetry. In general, the motor current does not show strong signatures related to bearing fault as discussed in Section II so the signatures related to magnetic asymmetry are all very low at noise floor level in current and hard to observe.

VI. CONCLUSION

In this paper, it is shown that stray flux enables highly reliable bearing fault detection. The inherent asymmetry of the magnets is deployed to define new set of fault signature in stray magnetic flux together with the characteristic bearing signatures. The fault signatures in two PM motors with different degree of magnetic asymmetry are verified in simulations and validated with extensive experiments. The signatures in flux are consistent irrespective of control loop action and load effects which are essential for condition monitoring. It is also shown that the bearing fault signature in stator current is not consistent throughout the operating region. It is affected both by the closed loop control action of microcontroller and loading effects. This makes flux-based detection superior to the current based detection. The advantage of locating the faulty bearing with the proposed stray flux-based method expedite the maintenance process. As the proposed fault detection method has high SNR, effective in all the operating conditions and uses low cost sensor, it can be considered as better alternative for the detection of bearing fault in permanent magnet motors.

REFERENCES

[1] "Report of large motor reliability survey of industrial and commercial installations, Part I," *IEEE Trans. Ind. Appl.*, vol. IA-21, no. 4, pp. 853–864, Jul. 1985.

[2] M. Pacas, S. Villwock, and R. Dietrich, "Bearing damage detection in permanent magnet synchronous machines," in *Proc. IEEE Energy Convers. Congr. Expo.*, Sep. 2009, pp. 1098–1103.

[3] F. Immovilli, A. Bellini, R. Rubini, and C. Tassoni, "Diagnosis of bearing faults in induction machines by vibration or current signals: A critical comparison," *IEEE Trans. Ind. Appl.*, vol. 46, no. 4, pp. 1350–1359, Jul. 2010.

[4] K. Kudelina, B. Asad, T. Vaimann, A. Rassolkin, and A. Kallaste, "Effect of bearing faults on vibration spectrum of BLDC motor," in *Proc. IEEE Open Conf. Electr., Electron. Inf. Sci. (eStream)*, Apr. 2020, pp. 1–6.

[5] C. Bianchini, F. Immovilli, M. Cocconcelli, R. Rubini, and A. Bellini, "Fault detection of linear bearings in brushless AC linear motors by vibration analysis," *IEEE Trans. Ind. Electron.*, vol. 58, no. 5, pp. 1684–1694, May 2011.

[6] A. K. Samanta, A. Routray, S. R. Khare, and A. Naha, "Minimum distance-based detection of incipient induction motor faults using Rayleigh quotient spectrum of conditioned vibration signal," *IEEE Trans. Instrum. Meas.*, vol. 70, pp. 1–11, 2021.

[7] R. R. Schoen, T. G. Habetler, F. Kamran, and R. G. Bartfield, "Motor bearing damage detection using stator current monitoring," *IEEE Trans. Ind. Appl.*, vol. 31, no. 6, pp. 1274–1279, Dec. 1995.

[8] D. T. Hoang and H. J. Kang, "A motor current signal-based bearing fault diagnosis using deep learning and information fusion," *IEEE Trans. Instrum. Meas.*, vol. 69, no. 6, pp. 3325–3333, Jun. 2020.

[9] V. C. M. N. Leite, J. G. Borges da Silva, G. F. C. Veloso, L. E. B. da Silva, G. Lambert-Torres, E. L. Bonaldi, and L. E. de Lacerda de Oliveira, "Detection of localized bearing faults in induction machines by spectral kurtosis and envelope analysis of stator current," *IEEE Trans. Ind. Electron.*, vol. 62, no. 3, pp. 1855–1865, Mar. 2015.

[10] M. Blodt, D. Bonacci, J. Regnier, M. Chabert, and J. Faucher, "On-line monitoring of mechanical faults in variable-speed induction motor drives using the Wigner distribution," *IEEE Trans. Ind. Electron.*, vol. 55, no. 2, pp. 522–533, Feb. 2008.

[11] T. G. Habetler, "Current-based motor condition monitoring: Complete protection of induction and PM machines," in *Proc. Int. Aegean Conf. Electr. Mach. Power Electron.*, Sep. 2007, pp. 378–384.

[12] T. Goktas, M. Zafarani, K. W. Lee, B. Akin, and T. Sculley, "Comprehensive analysis of magnet defect fault monitoring through leakage flux," *IEEE Trans. Magn.*, vol. 53, no. 4, pp. 1–10, Apr. 2017.

[13] Y. Park, C. Yang, J. Kim, H. Kim, S. B. Lee, K. N. Gyftakis, P. A. Panagiotou, S. H. Kia, and G.-A. Capolino, "Stray flux monitoring for reliable detection of rotor faults under the influence of rotor axial air ducts," *IEEE Trans. Ind. Electron.*, vol. 66, no. 10, pp. 7561–7570, Oct. 2019.

[14] V. Gurusamy, E. Bostanci, C. Li, Y. Qi, and B. Akin, "A stray magnetic flux-based robust diagnosis method for detection and location of inter-turn short circuit fault in PMSM," *IEEE Trans. Instrum. Meas.*, vol. 70, pp. 1–11, 2021.

[15] T. Goktas, M. Arkan, M. S. Mamis, and B. Akin, "Broken rotor bar fault monitoring based on fluxgate sensor measurement of leakage flux," in *Proc. IEEE Int. Electr. Mach. Drives Conf. (IEMDC)*, May 2017, pp. 1–6.

[16] M. Negrea, P. Jover, and A. Arkkio, "Electromagnetic flux-based condition monitoring for electrical machines," in *Proc. 5th IEEE Int. Symp. Diag. Electr. Mach., Power Electron. Drives*, Sep. 2005, pp. 1–6.

[17] O. Vitek, M. Janda, V. Hajek, and P. Bauer, "Detection of eccentricity and bearings fault using stray flux monitoring," in *Proc. 8th IEEE Symp. Diag. Electr. Mach., Power Electron. Drives*, Sep. 2011, pp. 456–461.

[18] L. Frosini, C. Harlisca, and L. Szabo, "Induction machine bearing fault detection by means of statistical processing of the stray flux measurement," *IEEE Trans. Ind. Electron.*, vol. 62, no. 3, pp. 1846–1854, Mar. 2015.

[19] M. A. Khan, I. Husain, M. R. Islam, and J. T. Klass, "Design of experiments to address manufacturing tolerances and process variations influencing cogging torque and back EMF in the mass production of the permanent-magnet synchronous motors," *IEEE Trans. Ind. Appl.*, vol. 50, no. 1, pp. 346–355, Jan. 2014.

[20] S. Zhang, B. Wang, M. Kanemaru, C. Lin, D. Liu, M. Miyoshi, K. H. Teo, and T. G. Habetler, "Model-based analysis and quantification of bearing faults in induction machines," *IEEE Trans. Ind. Appl.*, vol. 56, no. 3, pp. 2158–2170, May 2020.

[21] M. Blodt, P. Granjon, B. Raison, and G. Rostaing, "Models for bearing damage detection in induction motors using stator current monitoring," *IEEE Trans. Ind. Electron.*, vol. 55, no. 4, pp. 1813–1822, Apr. 2008.

[22] *DRV425 Fluxgate Magnetic-Field Sensor Datasheet*. Accessed: Feb. 2021. [Online]. Available: https://www.ti.com/lit/gpn/drv425

[23] *LEM Current Sensor Datasheet*. Accessed: Feb. 2021. [Online]. Available: https://www.lem.com/sites/default/files/products_datasheets/hx_03_50-p_ver15.pdf

[24] M. Zafarani, T. Goktas, B. Akin, and S. E. Fedigan, "Modeling and dynamic behavior analysis of magnet defect signatures in permanent magnet synchronous motors," *IEEE Trans. Ind. Appl.*, vol. 52, no. 5, pp. 3753–3762, Sep. 2016.

[25] B. Corne, B. Vervisch, S. Derammelaere, S. M. A. Cruz, J. Knockaert, and J. Desmet, "Single point outer race bearing fault severity estimation using stator current measurements," in *Proc. IEEE Int. Electric Mach. Drives Conf. (IEMDC)*, May 2017, pp. 1–7.

[26] O. Zandi and J. Poshtan, "Fault diagnosis of brushless DC motors using built-in Hall sensors," *IEEE Sensors J.*, vol. 19, no. 18, pp. 8183–8190, Sep. 2019.

VIGNESHWARAN GURUSAMY (Graduate Student Member, IEEE) received the B.Tech. degree in electrical and electronics engineering from SASTRA University, Thanjavur, India, in 2012, and the M.S. degree in electrical engineering from The University of Texas at Dallas, Richardson, TX, USA, in 2018, where he is currently pursuing the Ph.D. degree. From 2012 to 2016, he was an Electrical Machine Design Engineer with Lucas-TVS, an auto electrical company, Chennai, India. Since 2016, he has been with the Power Electronics and Drives Laboratory, The University of Texas at Dallas. His current research interests include fault diagnosis of electrical machines and design of electromechanical devices, like electrical machines and medium frequency transformers.

KUDRA H. BARUTI (Student Member, IEEE) received the bachelor's degree in electrical and electronics engineering from Istanbul Okan University, Turkey, in 2015. He is currently pursuing the Ph.D. degree in electrical engineering with the Power Electronics and Drives Laboratory, The University of Texas at Dallas. His research interests include self-commissioning, and control and fault diagnosis of electric machines.

MOHSEN ZAFARANI (Member, IEEE) received the M.S. degree in electrical engineering from the Isfahan University of Technology, Isfahan, Iran, in 2011, and the Ph.D. degree in electrical engineering from The University of Texas at Dallas, Dallas, TX, USA, in 2018. In 2018, he joined Delphi Technologies, as an Electrical Design Engineer and worked on power electronic high-voltage inverters and dc–dc converters for automotive industries. Since January 2020, he has been working as a Senior Design Engineer with ASML Company, Veldhoven, The Netherlands, working on the electromagnetic design of actuators. He is also working on power electronic converters, such as inverters and dc–dc converters for automotive industries. His research interests include design and analysis of electric machines, modeling of electromagnetic devices, and fault diagnoses in PM motors.

WAI LEE received the bachelor's, M.S., and Ph.D. degrees from the Massachusetts Institute of Technology (MIT). He is currently a TI Fellow with Texas Instruments and the Chief Technologist of the sensor products business. He has authored or coauthored about 40 journal publications in IEEE and APS journals. He has given over 20 conference presentations at various IEEE conferences and given invited talks at leading universities around the world, including MIT and Tsinghua University. He has also served on technical program committees for a number of premium International conferences.

BILAL AKIN (Senior Member, IEEE) received the Ph.D. degree in electrical engineering from Texas A&M University, College Station, TX, USA, in 2007. From 2005 to 2008, he was a Research and Development Engineer with Toshiba Industrial Corporation, Houston, TX, USA. From 2008 to 2012, he worked as a Research and Development Engineer with C2000 DSP Systems, Texas Instruments Inc. Since 2012, he has been a Faculty Member with The University of Texas at Dallas, Richardson, TX, USA. His research interests include design, control, and diagnosis of electric motors and drives, digital power control and management, and fault diagnosis and condition monitoring of power electronics components and ac motors. He was a recipient of the NSF CAREER'15 Award, the IEEE TRANSACTIONS ON INDUSTRY APPLICATIONS First Place Prize Paper Award, the Top Editors Recognition Award from the IEEE TVT Society, the Jonsson School Faculty Research Award twice, and the Jonsson School Faculty Teaching Award. He is currently an Associate Editor of the IEEE TRANSACTIONS ON INDUSTRY APPLICATIONS and IEEE TRANSACTIONS ON VEHICULAR TECHNOLOGY.